Phase Relations and Gibbs Energies in the System Mn-Rh-O

K.T. JACOB and M.V. SRIRAM

Phase relations in the system Mn-Rh-O are established at 1273 K by equilibrating different compositions either in evacuated quartz ampules or in pure oxygen at a pressure of 1.01×10^5 Pa. The quenched samples are examined by optical microscopy, X-ray diffraction, and energy-dispersive X-ray analysis (EDAX). The alloys and intermetallics in the binary Mn-Rh system are found to be in equilibrium with MnO. There is only one ternary compound, $MnRh_2O_4$, with normal spinel structure in the system. The compound Mn_3O_4 has a tetragonal structure at 1273 K. A solid solution is formed between $MnRh_2O_4$ and Mn_3O_4. The solid solution has the cubic structure over a large range of composition and coexists with metallic rhodium. The partial pressure of oxygen corresponding to this two-phase equilibrium is measured as a function of the composition of the spinel solid solution and temperature. A new solid-state cell, with three separate electrode compartments, is designed to measure accurately the chemical potential of oxygen in the two-phase mixture, Rh + $Mn_{3-2x}Rh_{2x}O_4$, which has 1 degree of freedom at constant temperature. From the electromotive force (emf), thermodynamic mixing properties of the Mn_3O_4-$MnRh_2O_4$ solid solution and Gibbs energy of formation of $MnRh_2O_4$ are deduced. The activities exhibit negative deviations from Raoult's law for most of the composition range, except near Mn_3O_4, where a two-phase region exists. In the cubic phase, the entropy of mixing of the two Rh^{3+} and Mn^{3+} ions on the octahedral site of the spinel is ideal, and the enthalpy of mixing is positive and symmetric with respect to composition. For the formation of the spinel (sp) from component oxides with rock salt (rs) and orthorhombic (orth) structures according to the reaction, MnO (rs) + Rh_2O_3 (orth) → $MnRh_2O_4$ (sp),

$$\Delta G^\circ = -49{,}680 + 1.56T\ (\pm 500)\ \text{J mol}^{-1}$$

The oxygen potentials corresponding to MnO + Mn_3O_4 and Rh + Rh_2O_3 equilibria are also obtained from potentiometric measurements on galvanic cells incorporating yttria-stabilized zirconia as the solid electrolyte. From these results, an oxygen potential diagram for the ternary system is developed.

I. INTRODUCTION

THERE is currently much interest in the compound $MnRh_2O_4$ and the spinel solid solution $Mn_{3-2x}Rh_{2x}O_4$ for catalytic applications. A partial phase diagram for the system Mn-Rh-O at 1373 K has been proposed by Schmahl *et al.*[1] They indicate a complete range of solid solution between Mn_3O_4 with tetragonal structure and $MnRh_2O_4$ with cubic structure, which cannot be valid. The purpose of this study is to establish a complete isothermal section of the ternary phase diagram at 1273 K and to measure thermodynamic properties of ternary oxide phases as a function of composition and temperature. The phase diagram is established by identification of phases present in equilibrated samples. The different compositions are prepared by mixing metals, alloys, and oxides in different proportions. The samples containing only oxides in their highest oxidation state are equilibrated in pure oxygen. Samples containing alloys and lower-valent oxides are equilibrated in evacuated quartz ampules to avoid oxidation. The sample is contained in a zirconia crucible placed inside the quartz ampule. Isothermal equilibration studies are supplemented by differential thermal analysis (DTA) runs on $Mn_{3-2x}Rh_{2x}O_4$ solid solutions, for small values of x.

After establishing phase relations in the system Mn-Rh-O, a solid-state galvanic cell is designed to measure the thermodynamic properties of ternary oxide phases. Because of the nature of phase relations in the Mn-Rh-O system, Gibbs energy of formation of $MnRh_2O_4$ cannot be directly obtained from electromotive force (emf) measurement involving three-phase equilibria. The Gibbs energy of formation is derived from measurements on spinel solid solutions. The solid solutions exist with metallic rhodium. The two-phase region has associated with it 1 degree of freedom at constant temperature. The composition of the spinel changes during emf measurement of the oxygen chemical potential because of electrochemical permeability of the solid electrolyte. A special galvanic cell, incorporating three compartments, is designed to overcome this problem. In addition to the usual measuring and reference electrodes, a third buffer electrode is introduced which acts as a sink for the flux of oxygen.

A modified form of the Gibbs-Duhen relation is developed for deriving the activity coefficients of $MnRh_2O_4$ and Mn_3O_4 from the variation of the equilibrium partial pressure of oxygen with composition of the spinel solid solution. The equilibrium constant for the reaction

K.T. JACOB, Chairman and Professor, Materials Research Center, and Professor, Department of Metallurgy, is with the Indian Institute of Science, Bangalore-560 012, India. M.V. SRIRAM, Student, is with the Department of Metallurgical Engineering, Indian Institute of Technology, Kanpur 208 016, India.

Manuscript submitted October 4, 1993.

represented by the tie lines is then derived from the oxygen partial pressure and activities in the solid solution. The standard Gibbs free energy of formation of $MnRh_2O_4$ is obtained by combining the results with the auxiliary data on Mn_3O_4. The oxygen potentials corresponding to mixtures of MnO + Mn_3O_4 and Rh + Rh_2O_3 are redetermined to check values reported in the literature. Based on these results, an oxygen potential diagram is developed for the ternary system at 1273 K.

II. PHASE DIAGRAM STUDIES

A. *Materials*

The starting materials are powders of Mn, Rh, $MnSO_4$, and Rh_2O_3 of purity greater than 99.9 pct. The compound Mn_3O_4 is prepared by heating $MnSO_4$ gradually in flowing argon gas to a temperature of 1300 K for 20 ks. The apple-green MnO is prepared by hydrogen reduction of Mn_3O_4 kept in a platinum boat at 1225 K. Alloys rich in manganese are made by induction melting together rhodium sponge and manganese flakes of 99.9 pct purity in stabilized zirconia crucibles under a stream of prepurified argon. Alloys rich in rhodium are obtained by arc melting rhodium sponge and an equiatomic Mn-Rh alloy on a water-cooled copper hearth under argon cover.

The argon gas is 99.999 pct pure and is further purified by passing through Cu_2O at 850 K to oxidize residual CO to CO_2 and H_2 to H_2O. The CO_2 is then absorbed by passing through a column of NaOH. The gas is dried by silica gel, magnesium perchlorate, and phosphorus pentoxide. Finally, the residual oxygen in argon is removed by passing through columns containing copper wool at 723 K and titanium granules at 1173 K.

B. *Procedure*

The phase relations are explored by equilibrating mixtures of different elements or compounds at 1273 K, followed by quenching in liquid nitrogen or chilled mercury and phase identification. Thirty ternary compositions are equilibrated for periods up to 5×10^5 s. The samples are quenched, ground, and repelletized twice during this period. Phase composition of the samples is found to be unaltered by further heat treatment. The overall composition of the samples studied is shown on the Gibbs triangle of Figure 1.

Two arrangements are used for equilibrating samples at high temperature. Several mixtures containing Mn_3O_4, $MnRh_2O_4$, and Rh_2O_3 are heat-treated in a stream of pure oxygen at a pressure of 1.01×10^5 Pa, using an apparatus described earlier.[2] The mixtures are pelletized and contained in zirconia crucibles. Several compositions along the pseudo-binary Mn_3O_4-$MnRh_2O_4$ are examined. After equilibration, the samples are quenched in liquid nitrogen or chilled mercury. The mass of each sample is determined before and after equilibration.

Mixtures containing Mn, Rh, Mn-Rh alloys, and MnO are equilibrated in evacuated quartz ampules to prevent oxidation. The pellets made from each mixture are contained in a zirconia crucible, placed inside the quartz ampule. After the heat treatment, the ampules are quenched in chilled mercury. The phases present in the samples are identified by optical microscopy, X-ray diffraction, and energy-dispersive X-ray analysis (EDAX). Pure Mn, Rh, MnO, and Rh_2O_3 are used as standards for EDAX. Differential thermal analysis is done in air for $Mn_{3-2x}Rh_{2x}O_4$ solid solutions with $X = 0.01$, 0.025, 0.05, 0.10, and 0.15 to locate the two-phase field between tetragonal Mn_3O_4 and cubic $MnRh_2O_4$.

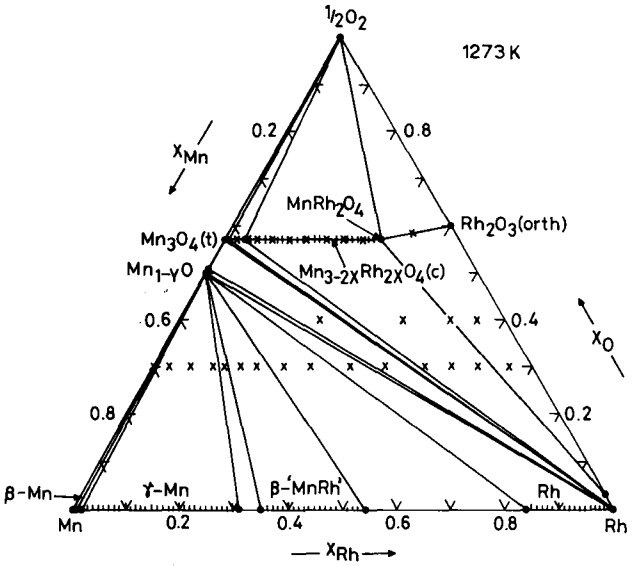

Fig. 1 — Phase relations in the system Mn-Rh-O at 1273 K. The composition of the samples analyzed is shown by X.

C. *Results and Discussion*

Samples initially containing a mixture of Mn_3O_4 and Rh_2O_3 are found to lose mass during equilibration in pure oxygen gas. However, samples consisting of Mn_3O_4 and $MnRh_2O_4$ or $MnRh_2O_4$ and Rh_2O_3 do not exhibit a loss in mass. This suggests partial reduction of Mn_3O_4 and its reaction with Rh_2O_3 to form $MnRh_2O_4$, in samples containing Mn_3O_4 and Rh_2O_3.

The equilibrium phase diagram for the system Mn-Rh-O at 1273 K, composed from the results of this study, is shown in Figure 1. Only one oxide, Rh_2O_3, is found along the Rh-O binary, and two oxides, $Mn_{1-y}O$ and Mn_3O_4, on the Mn-O join. There are six phase fields in which three condensed phases coexist. All the metallic phases are in equilibrium with essentially stoichiometric MnO. The β-Mn solid solution exists for $1.00 > X_{Mn} > 0.992$. A solid solution with γ-Mn structure is present for $0.982 > X_{Mn} > 0.69$. The intermetallic compound "MnRh" has an extensive homogeneity range, $0.65 > X_{Mn} > 0.46$. The solid solubility of manganese in rhodium extends up to $X_{Mn} = 0.16$ at 1273 K. The phase diagram for the binary Mn-Rh system is not fully established. The phase boundaries obtained in this study at 1273 K agree within ±2 at. pct with the tentative values suggested in the recent compilation edited by Massalski.[3] The oxides $Mn_{1-y}O$ and Mn_3O_4 coexist with rhodium. The solid solution, $Mn_{3-2x}Rh_{2x}O_4$, is also in equilibrium with rhodium metal. The solubility of rhodium in $Mn_{1-y}O$, Mn_3O_4, and $Mn_{3-2x}Rh_{2x}O_4$ is not detectable (<0.1 mol pct).

There is extensive solid solubility between Mn_3O_4 and $MnRh_2O_4$. The structure is tetragonal for $1.00 > X_{Mn_3O_4} > 0.975$ and cubic for $0.88 > X_{Mn_3O_4} > 0.00$. In between, there is a two-phase region along the Mn_3O_4-$MnRh_2O_4$ join. Differential thermal analysis scan of the $Mn_{3-2x}Rh_{2x}O_4$ solid solutions indicates that this two-phase field narrows with increasing temperature. At 1373 K, the two-phase field is confined between $X_{Mn_3O_4} = 0.988$ and 0.95. It is therefore understandable why the two-phase field was missed by Schmahl *et al.*,[1] who did not probe this region in detail. There appears to be a small solubility (~1 mol pct) of Rh_2O_3 in $MnRh_2O_4$. There is no serious conflict between the complete phase diagram for the Mn-Rh-O system at 1273 K developed in this study and the partial diagram at 1373 K proposed by Schmahl *et al.*[1]

III. THERMODYNAMIC MEASUREMENTS

A. *Outline of the Method*

Because of the nature of phase relations in the system Mn-Rh-O, the standard free energy of formation of $MnRh_2O_4$ cannot be obtained from the measurement of the partial pressure of oxygen corresponding to an equilibrium between three condensed phases. The alternative available is to measure the chemical potential of oxygen corresponding to the equilibrium between metallic rhodium and the solid solution $Mn_{3-2x}Rh_{2x}O_4$. This two-phase equilibrium is bivariant. At constant temperature, the system has 1 degree of freedom. The chemical potential of oxygen will vary with composition of the solid solution under isothermal conditions. The partial pressure of oxygen is defined by the reaction

$$3(MnRh_2O_4)_{(ss)} \rightleftarrows (Mn_3O_4)_{(ss)} + 6\,Rh + 4O_2 \quad [1]$$

for which

$$\Delta G_1^\circ = -RT \ln K_1 = -RT \ln \frac{a_{Mn_3O_4} \cdot P_{O_2}^4}{a_{MnRh_2O_4}^3} \quad [2]$$

The oxygen partial pressure corresponding to each tie line in the two-phase region is proportional to the fourth root of the ratio $(a_{MnRh_2O_4}^3/a_{Mn_3O_4})$ of activities in the solid solution. To obtain the individual activities or activity coefficients of components of the solid solution, the variation of the partial pressure of oxygen with composition has to be measured. The activity coefficients can then be derived by integrating a function containing the partial pressure of oxygen between prescribed limits of composition, using a modified form of the Gibbs–Duhem relation.[4] From a knowledge of activity coefficients, tie lines, and corresponding partial pressures, the Gibbs energy of formation of $MnRh_2O_4$ can be obtained.

Electrochemical techniques for the measurement of oxygen potential of an invariant system at constant temperature are well established.[5] However, measurements on systems that have 1 or more degrees of freedom are more difficult, especially if the phases involved are solids. Since the time required for the attainment of equilibrium in such cases is rather long, the oxygen potential of the gas and, consequently, the composition of the solid may be altered by minor perturbations such as oxygen leakage, both physical and electrochemical.[6] When the electrode contains a liquid phase, equilibration is more rapid, and the drift in emf during measurement is less significant.

Initial measurements on two-phase equilibria represented by Reaction [1], using the conventional two-compartment arrangement[7] with physical separation of the two electrodes by a long solid electrolyte tube, have not been successful. The emf is found to drift gradually with time. The drift is reduced when a sealed system, suggested by Charette and Flengas,[8] is employed. However, the drift cannot be suppressed completely. Therefore, a new design, with three separate electrode compartments, is developed for measurements on systems that have 1 or more degrees of freedom. The oxygen potentials corresponding to the equilibrium between $Mn_{1-y}O + Mn_3O_4$ and $Rh + Rh_2O_3$ are also measured using the new design to check values reported in the literature.[8–14]

B. *Design of Galvanic Cell with Three Compartments*

1. *Principle*

The cell design used for high-temperature emf measurements is shown in Figure 2. It consists of three distinct compartments, separated by two impervious yttria-stabilized zirconia tubes, each closed at one end. The cell can be represented schematically as follows:

Pt-Rh, $O_2(P'_{O_2})$ measuring electrode	$\|\|$	$(Y_2O_3)ZrO_2$	$\|\|$	$O_2(P''_{O_2})$ buffer electrode $P''_{O_2} \approx P'_{O_2}$	$\|\|$	$(Y_2O_3)ZrO_2$	$\|\|$	$O_2(P'''_{O_2})$, Pt-Rh reference electrode

[3]

The measuring and reference electrodes are contained inside each zirconia tube. When the difference in the chemical potential of oxygen between these electrodes is substantial, there is always a small flux of oxygen through the zirconia electrolyte separating them, even in the absence of physical porosity.[6] The electrochemical permeability is caused by the coupled transport of oxygen ions and electrons or holes in the solid electrolyte under the oxygen potential gradient. This flow of oxygen can be stopped only by opposing it with an external DC voltage equivalent to the oxygen chemical potential difference.[15]

If an electrode consists of a chemically invariant system at constant temperature and pressure, and electrode reactions are sufficiently rapid, the semipermeability flux of oxygen does not generally alter its chemical potential. Experimentally, the effect of the semipermeability flux on emf can be minimized by taking a greater amount of the phase that is consumed by the flux at each of the solid electrodes.[16] However, when the electrode system is static and has 1 or more degrees of freedom, the flux of oxygen will change its composition and potential, at least near the electrode/electrolyte interface. The third compartment introduced between the measuring and reference electrodes acts as a sink for the flux and prevents it from reaching the measuring electrode. By design, the buffer electrode has an oxygen potential equal to or very slightly lower than that of the

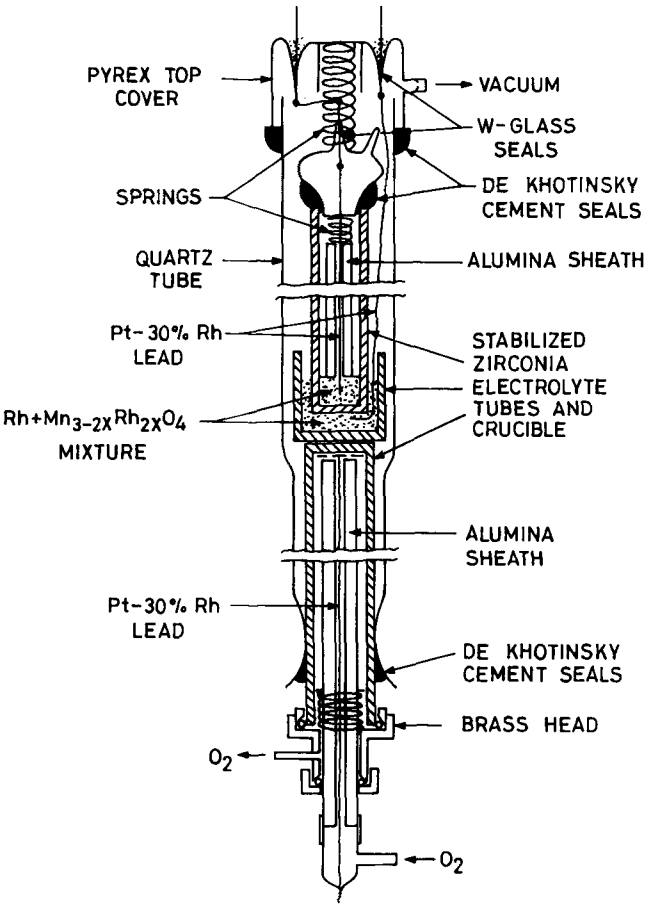

Fig. 2—Schematic diagram of the three-electrode system for emf measurement.

measuring electrode. There is no effective difference in chemical potential between the measuring electrode and the buffer. In the absence of a driving force for transport of oxygen, the measuring electrode remains unpolarized, and its chemical potential and concentration are unaltered.

Since the chemical potential of the reference electrode is generally different from that of the buffer, there is transport of oxygen between these electrodes through the solid electrolyte. If the thermodynamic capacity[17] of the buffer electrode is high, it will be able to absorb the flux without significantly altering its chemical potential. A nonpolarizable reference electrode, whose chemical potential is not altered by the electrochemical flux of oxygen, is necessary for accurate measurement. Pure oxygen flowing over a platinized surface of zirconia electrolyte, at a pressure of 1.01×10^5 Pa and high temperature, constitutes the primary standard for oxygen potential and forms a nonpolarizable electrode.

The buffer electrode concept has been suggested recently by Lundberg and Rosén.[18] However, in their design, a solid reference electrode is used, which may become polarized if the kinetics of reactions at this electrode are sluggish. The idea of deflecting the electrochemical flux is inspired by the zirconia point-electrode configuration suggested by Fouletier *et al.*[6] The triple electrode-bielectrolyte cell design used by Mallika *et al.*,[19] incorporating a point electrode, is less satisfactory because the buffer electrode has an intermediate chemical potential. The point electrode is used in their design to reduce the flux of oxygen by reducing the contact area, but not to deflect the flux from the measuring electrode. A major disadvantage of their design is that both the buffer and the measuring electrodes are exposed to a common gas phase. The transfer of oxygen between the electrodes *via* the gas, mediated by the presence of trace concentrations of H_2O, CO, and CO_2, can significantly affect the emf measurement.

2. *Apparatus and procedure*

The introduction of the third compartment renders the construction of the galvanic cell more difficult. Moreover, in the system under study, the partial pressure of oxygen is quite appreciable, especially at the higher temperatures. Therefore, the static sealed design used by Charette and Flengas[8] is more appropriate than other designs which employ either dynamic vacuum or inert gas flow.[5,7]

In studies on spinel solid solutions, the measuring electrode consists of an intimate mixture of Rh and $Mn_{3-2x}Rh_{2x}O_4$ powders in equimolar ratio. The mixture is rammed against the closed end of a stabilized zirconia tube with a Pt-30 pct Rh lead embedded in the mixture. An alumina sheath is used to insulate this lead and to press the measuring electrode against the zirconia tube. The top of the zirconia tube is closed with a tight-fitting bell-shaped PYREX* tube, which supports a tungsten electrode connection sealed into the glass. The joint between the bell and the zirconia tube is sealed with De Khotinsky cement. A spring placed between the bell and the alumina sheath applies pressure on the measuring electrode. The assembled measuring electrode half-cell is first evacuated using a side arm tube shown in the diagram, heated to ~400 K, and then the tube is flame scaled under vacuum.

*PYREX is a trademark of Corning Glass Works, Corning, NY.

The measuring half-cell assembly rests on a buffer electrode contained in a stabilized-zirconia crucible. For measurements on spinel solid solutions, the buffer also consists of a mixture of Rh and $Mn_{3-2x}Rh_{2x}O_4$, but the spinel phase is slightly richer in Mn_3O_4 than the measuring electrode. Thus, the partial pressure of oxygen in the buffer is slightly less (~15 mV equivalent) than that of the measuring electrode at the start of the experiment. However, in the course of the experiment, partial pressure of the buffer increases to a value equivalent of 15 mV higher than that of the measuring electrode, because of the oxygen flux from the reference side. The buffer electrode is prepared by consolidating an intimate equimolar mixture of constituent phases in the zirconia crucible, with a Pt-30 pct Rh lead embedded in the powder.

The zirconia crucible rests on another inverted zirconia tube. The mating surfaces of the crucible and tube are polished with diamond paste to minimize resistance. The inside surface of the inverted zirconia tube is platinized. A platinum gauze is pressed against the closed end of the inverted tube, using an alumina sheath. A Pt-30 pct Rh lead, spot welded to the gauze, passes through the alumina sheath. The open end of the inverted zirconia tube is fitted with a brass head. Pure oxygen

gas at a pressure of 1.01×10^5 Pa is flowed through the inverted zirconia tube at a rate of 3 mL s^{-1}. The pressure inside the tube is controlled by a cascade of bubblers placed at the gas exit. The oxygen electrode serves as the reference.

The cell is assembled inside a fused quartz enclosure. The inverted zirconia tube containing the reference electrode is first fixed inside the vertical quartz enclosure with De Khotinsky cement. The zirconia crucible containing the buffer electrode is placed on top of the inverted tube. The measuring electrode assembly is then loaded into the crucible. The annular space between the zirconia tube and crucible is filled with the buffer electrode mixture. The measuring electrode assembly is pressed down by means of a second metal spring between the bell and the top PYREX cover. The top cover supports two platinum-glass seals through which electrical connections are made. All electrode connections are silver soldered. Finally, the top cover is cemented in place by melting the De Khotinsky cement in the ring container shown in the diagram. The cement is allowed to solidify while pressing the top cover against the spring. Then the outer quartz enclosure is also evacuated from a side arm tube and flame sealed under vacuum. The top half of the cell assembly, shown in Figure 2, is identical to that developed by Charette and Flengas.[8]

The entire assembly shown in Figure 2 is placed inside a vertical resistance furnace, with the electrodes located in the even-temperature zone (±1 K). The upper and lower parts of the assembly, where cement seals are located, remain at room temperature during measurement. A Faraday cage made from stainless steel foil was placed between the furnace and the cell assembly. The foil was grounded to minimize induced emf on cell leads. The temperature of the furnace was controlled to ±1 K. The temperature was measured by a Pt/Pt-13 pct Rh thermocouple, calibrated against the melting point of gold. The cell potentials were measured with a high-impedance digital voltmeter with a sensitivity of ±0.01 mV. The potential readings were corrected for small thermal emfs, measured separately.

Although the cell assembly shown in Figure 2 consists of three electrode compartments, the cell potential is determined only by the chemical potentials of oxygen in the measuring and reference electrodes. Thus, the effective cell can be concisely written as

$$\text{Pt-Rh, Rh} + \text{Mn}_{3-2x}\text{Rh}_{2x}\text{O}_4/(\text{Y}_2\text{O}_3)\text{ZrO}_2/\text{O}_2 \ (1.01 \times 10^5 \text{ Pa}), \text{Pt-Rh} \quad [4]$$

The cell is written such that the right electrode is positive. The oxygen potentials corresponding to Rh + Rh_2O_3 and MnO + Mn_3O_4 mixtures are determined using cells

$$\text{Pt-Rh, Rh} + \text{Rh}_2\text{O}_3/(\text{Y}_2\text{O}_3)\text{ZrO}_2/\text{O}_2(1.01 \times 10^5 \text{ Pa}), \text{Pt-Rh} \quad [5]$$

$$\text{Pt, Mn}_{1-y}\text{O} + \text{Mn}_3\text{O}_4/(\text{Y}_2\text{O}_3)\text{ZrO}_2/\text{O}_2 \ (1.01 \times 10^5 \text{ Pa}), \text{Pt} \quad [6]$$

The "three-electrode design" is also used for measurement on cells [5] and [6]. The measuring and buffer electrodes in cell [5] consist of an intimate mixture of Rh and Rh_2O_3 in the molar ratio 2:1. Similarly, a mixture of MnO and Mn_3O_4 in the molar ratio 2:1 is used in cell [6]. Minor alterations in these mixing ratios do not affect the emf. The oxygen potentials corresponding to the equilibria between Mn-Rh alloys or intermetallics and MnO are not measured, since they fall outside the electrolytic conduction domain of the solid electrolyte $(Y_2O_3)ZrO_2$. X-ray diffraction analysis of the electrodes before and after each experiment indicates negligible change in their phase composition.

C. *Results and Discussion*

1. *Activities in the Mn_3O_4-$MnRh_2O_4$ solid solution*

The reversible emf of cell [4] is shown as a function of temperature in Figure 3 for different compositions of the oxide solid solution. The reversibility of the emf is established by microcoulometric titration in both directions. A small quantity of current (~50 μA) is passed through the cell, using an external potential source for ~300 s, and the open-circuit emf is subsequently monitored as a function of time. The emf is found to return to the steady value before each titration. During each titration, the chemical potential of oxygen at each electrode is displaced from equilibrium by an essentially infinitesimal amount. Since the electrodes return to the same potential after each displacement in opposite directions, equilibrium is presumed to be attained. The emf is not affected by the flow ratio of oxygen through

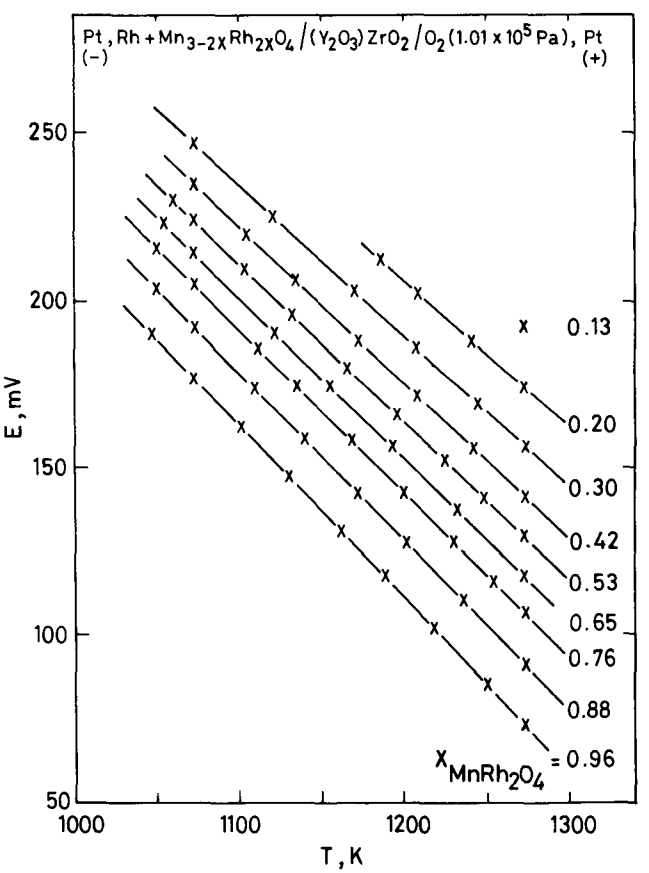

Fig. 3—Temperature dependence of the emf of cell [4] for different compositions of the solid solution.

the reference electrode in the range 2 to 5 mL s^{-1}. The emf is also found to be reproducible on temperature cycling in the range 1050 to 1273 K for most compositions. However, for $X = 0.20$, the emf is not reproducible below 1180 K. For $X = 0.13$, reversible emf is obtained only at 1273 K. For these compositions, the solid solution may not be homogeneous at lower temperatures and may separate into a mixture of tetragonal and cubic phases.

With the three-electrode design of the cell, the emfs are steady (±0.3 mV) for periods in excess of 30 ks. The buffer electrode contains a solid solution with the next lower concentration of $MnRh_2O_4$ than the measuring electrode. The emf of the buffer electrode against the reference is higher by 10 to 18 mV than that of the measuring electrode at the start of each experiment. As a consequence of the flux of oxygen from the reference electrode, the emf of the buffer electrode gradually decreases to a value ~15 mV lower than that of the measuring electrode by the end of the experiment. This clearly demonstrates the need for the buffer to absorb the oxygen flux and protect the measuring electrode from being disturbed. The emf of cell [4] is a linear function of temperature for each composition, as seen in Figure 3. The least-squares regression analysis of the emf gives coefficients listed in Table I.

In the temperature range of measurement shown in Figure 3, the solid solution $Mn_{3-2x}Rh_{2x}O_4$ has the cubic spinel structure, with practically all the Rh^{3+} and Mn^{3+} ions on the octahedral site. The cubic phase of Mn_3O_4 at 1473 K has a structure close to normal spinel, with ionic fraction of Mn^{3+} ions on the tetrahedral site less than 0.03.[20] This is consistent with the prediction from crystal field theory, which suggests a large octahedral site preference energy for Mn^{3+} ion (−95.4 kJ mol^{-1}) compared to Mn^{2+}, which has no preference between tetrahedral and octahedral sites.[21,22] It is known that $NiRh_2O_4$ has the normal structure,[23] despite the large octahedral site preference energy of Ni^{2+} ion (−86.2 kJ mol^{-1}).[21] Therefore, Rh^{3+} ion must have greater preference for the octahedral site than Ni^{2+} ion. These considerations suggest that in the solid solution between Mn_3O_4 and $MnRh_2O_4$, two ions of Mn^{3+} and Rh^{3+} mix on the octahedral site per formula unit. If the mixing is ideal, then activities of Mn_3O_4 and $MnRh_2O_4$ in the cubic phase would be equal to the square of their mole fractions. It is thus appropriate to define activity coefficients for the cubic phase as follows:

$$\gamma_{Mn_3O_4} = a_{Mn_3O_4}/(1 - X)^2 \quad [7]$$

$$\gamma_{MnRh_2O_4} = a_{MnRh_2O_4}/X^2 \quad [8]$$

where X represents the mole fraction of $MnRh_2O_4$. The equilibrium constant for Reaction [1] can be rewritten in terms of activity coefficients:

$$K_1 = \frac{\gamma_{Mn_3O_4}}{\gamma_{MnRh_2O_4}} \cdot \frac{(1 - X)^2 P_{O_2}^4}{X^6} \quad [9]$$

The Gibbs–Duhem equation for the Mn_3O_4-$MnRh_2O_4$ solid solution can be expressed as

$$X\, d \ln \gamma_{MnRh_2O_4} + (1 - X)\, d \ln \gamma_{Mn_3O_4} = 0 \quad [10]$$

Combining Eqs. [9] and [10],

$$d \ln \gamma_{MnRh_2O_4} = -\frac{(1 - X)}{(3 - 2X)} d \ln [f(X)] \quad [11]$$

where

$$f(X) = \frac{K_1 \cdot X^6}{(1 - X)^2 \cdot P_{O_2}^4} \quad [12]$$

Integrating Eq. [11] from $X = 1$ to $X = X$, one obtains

$$\ln \gamma_{MnRh_2O_4} = \int_1^X \frac{(1 - X)}{(3 - 2X)} d \ln \left(\frac{P_{O_2}^4 \cdot (1 - X)^2}{X^6} \right) \quad [13]$$

Similarly,

$$\ln \gamma_{Mn_3O_4} = \int_0^{(1-X)} -\frac{X}{(3 - 2X)} d \ln \left(\frac{P_{O_2} \cdot (1 - X)^2}{X^6} \right) \quad [14]$$

The evaluation of integrals for deriving the activity coefficient at 1273 K is illustrated in Figure 4. It is to be noted that as X varies from 0 to 1, $(1 - X)/(3 - 2X)$ ranges from 0.33 to 0, and $X/(3 - 2X)$ ranges from 0

Table I. Summary of emf Measurements on Rh + Mn_{3-2x} $Rh_{2x}O_4$ Mixtures

Composition $X_{MnRh_2O_4}$	emf, mV		
	$E = A + BT$	E_{1073K}	E_{1273K}
0.96	734.9 − 0.520T	176.9	72.9
0.88	734.2 − 0.505T	192.3	91.3
0.76	733.9 − 0.493T	204.9	106.3
0.65	732.3 − 0.483T	214.1	117.4
0.53	732.6 − 0.474T	224.0	129.2
0.42	732.8 − 0.465T	233.8	140.9
0.30	731.9 − 0.452T	246.8	156.5
0.20	730.0 − 0.437T	—	174.3
0.13	—	—	192.6

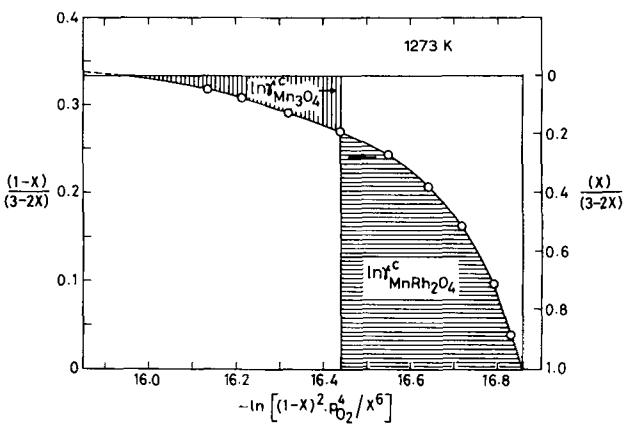

Fig. 4—Integration plot for deriving the activity coefficients of Mn_3O_4 and $MnRh_2O_4$. Separate vertical scales are provided for evaluating areas corresponding to the activity coefficient of each component.

to 1. Separate vertical scales are provided in Figure 4 for integrating Eqs. [13] and [14] graphically. The oxygen partial pressure corresponding to each tie line is obtained from the emf shown in Figure 3:

$$E = -\frac{RT}{\eta F} \ln (P_{O_2}/P^{\circ}_{O_2}) \qquad [15]$$

where E is the emf, F is the Faraday constant, R is the gas constant, T is the absolute temperature, $P^{\circ}_{O_2}$ is the standard pressure (1.01×10^5 Pa), and $\eta = 4$ is the number of electrons associated with each electrode reaction. The activity coefficients at 1273 K obtained by integration can be expressed by the relation

$$\frac{\ln \gamma_{MnRh_2O_4}}{(1-X)^2} = \frac{\ln \gamma_{Mn_3O_4}}{X^2} = 0.23\ (\pm 0.015) \qquad [16]$$

The activity coefficient evaluated at 1073 K can also be expressed by a similar relation with the value of the right-hand side equal to 0.27 (±0.02). These data suggest that the excess free energy of mixing of cubic Mn_3O_4 and $MnRh_2O_4$ is symmetric with respect to composition and independent of temperature, as follows:

$$\Delta G^E = 2435\ (\pm 200)\ X\ (1-X)\ \text{J mol}^{-1} \qquad [17]$$

This implies that the entropy of mixing is ideal and is given by

$$\Delta S = -2R\ [X \ln X + (1-X) \ln (1-X)] \qquad [18]$$

The entropy of mixing can be independently assessed from the temperature dependence of the emf of cell [4] shown in Figure 3. It can be readily shown that the partial excess entropy of mixing of $MnRh_2O_4$ is given by

$$\Delta S^E_{MnRh_2O_4} = 2\ R \ln X + \int_1^X \frac{4\eta F\ (1-X)}{(3-2X)}\, dB \qquad [19]$$

where $B = dE/dT$ is the temperature coefficient of emf. The partial entropy of $MnRh_2O_4$ obtained by integration is compared with the ideal value in Figure 5. The excess free energy of mixing appears to be dominated by the enthalpy contribution. The ionic radius of Mn^{3+} ion in the high spin state is 0.079 nm, and that of Rh^{3+} is 0.0805 nm in sixfold coordination, according to Shannon and Prewitt,[24,25] based on 0.119 nm as the radius of F^- ion. The small positive enthalpy of mixing is probably a consequence of the small difference in ionic radii.

At 1273 K, pure Mn_3O_4 is tetragonal. The activity coefficient of Mn_3O_4 given by Eq. [16] refers to cubic Mn_3O_4 as the standard state, since the data are obtained by integrating experimental information for cubic solid solutions. For calculating activities at 1273 K, the standard state is changed from cubic to tetragonal Mn_3O_4, using the data from Pankratz:[26]

$$Mn_3O_4\ (c) \rightarrow Mn_3O_4\ (t) \qquad [20]$$

$$\Delta G^{\circ} = -18{,}120 + 12.54T\ \text{J mol}^{-1} \qquad [21]$$

The composition dependence of activities in the Mn_3O_4 – $MnRh_2O_4$ solid solution at 1273 K, obtained from the results of this study, is shown in Figure 6.

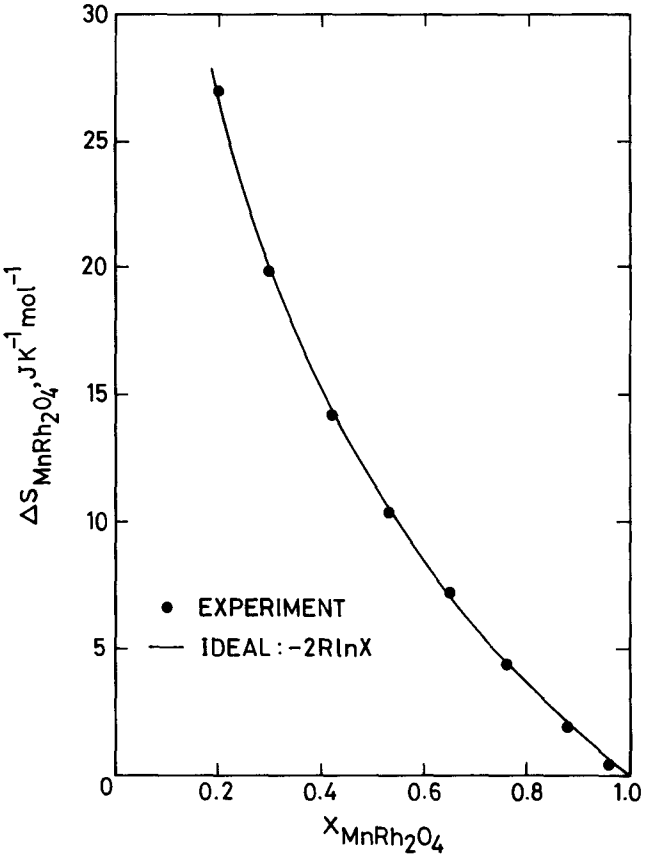

Fig. 5—Variation of the relative partial molar entropy of $MnRh_2O_4$ in the cubic spinel solid solution.

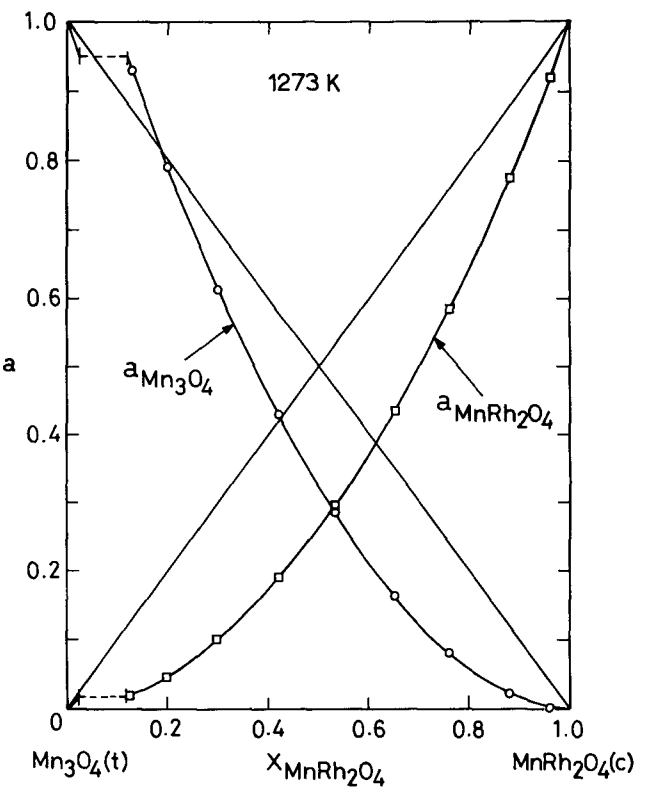

Fig. 6—Activity-composition relations in the system Mn_3O_4-$MnRh_2O_4$ at 1273 K.

2. *Gibbs energy of formation of $MnRh_2O_4$*

In deriving the activity coefficients in the oxide solid solution from the measured partial pressures of oxygen corresponding to tie lines in the two-phase region, Rh + $Mn_{3-2x}Rh_{2x}O_4$, a specific value for the equilibrium constant for Reaction [1] is not invoked. Use is made of the property $d \ln K_1 = 0$ at constant temperature. Therefore, the value of the equilibrium constant, K_1, can be derived from the oxygen partial pressure and activities of Mn_3O_4 and $MnRh_2O_4$ corresponding to each tie line. The average value of K_1 at 1273 K is 7.367 ($\pm$0.09) $\times$ 10^{-8} and 2.23 ($\pm$0.05) $\times$ 10^{-16} at 1073 K. Similar calculations are done at intermediate temperatures. The standard state for Mn_3O_4 in these calculations is the tetragonal form, which is more stable. The results can be expressed in terms of the standard free energy change for Reaction [1]:

$$\Delta G_1^\circ = 1{,}113{,}690 - 738.3T\ (\pm 250)\ \text{J mol}^{-1} \quad [22]$$

where the uncertainty limit corresponds to twice the standard error estimate. The value can be combined with the standard free energy of formation of Rh_2O_3 and the free energy for the oxidation of MnO to Mn_3O_4, obtained in the following sections, to calculate the free energy of formation of $MnRh_2O_4$ from component oxides. For the reaction

$$\text{MnO (rs)} + \text{Rh}_2\text{O}_3\ \text{(orth)} \rightarrow \text{MnRh}_2\text{O}_4\ \text{(sp)} \quad [23]$$

$$\Delta G_{23}^\circ = -49{,}680 + 1.56T\ (\pm 500)\ \text{J mol}^{-1} \quad [24]$$

The "second-law" enthalpy of formation of $MnRh_2O_4$ from component oxides at a mean temperature of 1173 K is $-$49.68 ($\pm$1.2) kJ mol^{-1}. The corresponding entropy of formation has a small value of $-$1.56 ($\pm$1) J mol^{-1} K^{-1}. For solid-state reactions, the entropy change is expected to be small. It would be useful to confirm this result by calorimetric studies on enthalpy of formation or heat capacity as a function of temperature.

3. *Gibbs energy of formation of Rh_2O_3*

The reversible emf of cell [5], measured using the three-electrode cell design, is plotted in Figure 7 as a function of temperature. The emf between the buffer electrode and the measuring electrode is found to vary from 0 at the beginning of the experiment to ~1 mV at the end of the experiment. Since the oxygen potential of the mixture Rh + Rh_2O_3 is invariant at constant temperature, the small electrochemical flux of oxygen does not appear to disturb the equilibrium significantly. Nevertheless, a small measurable polarization is present at high temperature. The numbers and letters in Figure 7 indicate the sequence of measurement. The least-squares regression analysis of the emf gives the relation

$$E = 684.6 - 0.487T\ (\pm 0.3)\ \text{mV} \quad [25]$$

X-ray diffraction patterns of the electrodes before and after each experiment indicate that Rh_2O_3 used in this study has the orthorhombic structure. The standard Gibbs free energy of formation of Rh_2O_3 obtained from the emf can be expressed as

$$\text{Rh (s)} + \frac{3}{2}\text{O}_2\ \text{(g)} \rightarrow \text{Rh}_2\text{O}_3\ \text{(orth)} \quad [26]$$

$$\Delta G_{26}^\circ = -396{,}365 + 282.0T\ (\pm 120)\ \text{J mol}^{-1} \quad [27]$$

The values obtained in this study are compared with earlier measurements[13,14] in Figure 8. Both the free energy and its temperature coefficient obtained in this study lie between values reported earlier by Kleykamp[13] at the lower end of the temperature scale, using a solid-state cell with Fe + FeO as the reference electrode, and by Schmahl and Minzl,[14] using a manometric technique at higher temperatures. The maximum difference between the values obtained in this study and Kleykamp[13] is 10 kJ mol^{-1} at 900 K. Unfortunately, accurate calorimetric data on Rh_2O_3 are not available for a more rigorous analysis of the free energy measurements.

4. *Oxygen potential corresponding to the coexistence of $Mn_{1-Y}O$ and Mn_3O_4*

The temperature dependence of the reversible emf of cell [6] is shown in Figure 9. At the beginning of the experiment, the emf between the buffer and measuring electrodes is found to be 0. There is a small increase in this emf to ~3.5 mV toward the end of the experiment. Therefore, the use of buffer electrode is recommended in future investigations of even invariant equilibria, especially when oxygen or air is used as the reference, and measured emf is large. The least-squares regression analysis of the emf yields the expression

$$E = 1{,}163 - 0.5821T\ (\pm 0.9)\ \text{mV} \quad [28]$$

The chemical potential of oxygen corresponding to the coexistence of $Mn_{1-Y}O$ and Mn_3O_4, computed from the emf, can be expressed by the relation

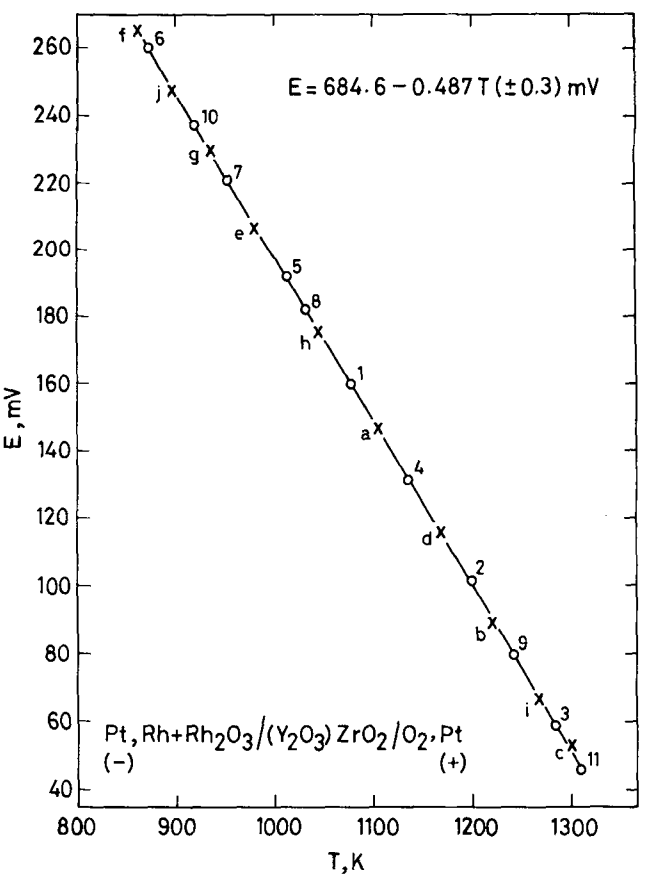

Fig. 7—Variation of the reversible emf of cell [5] with temperature.

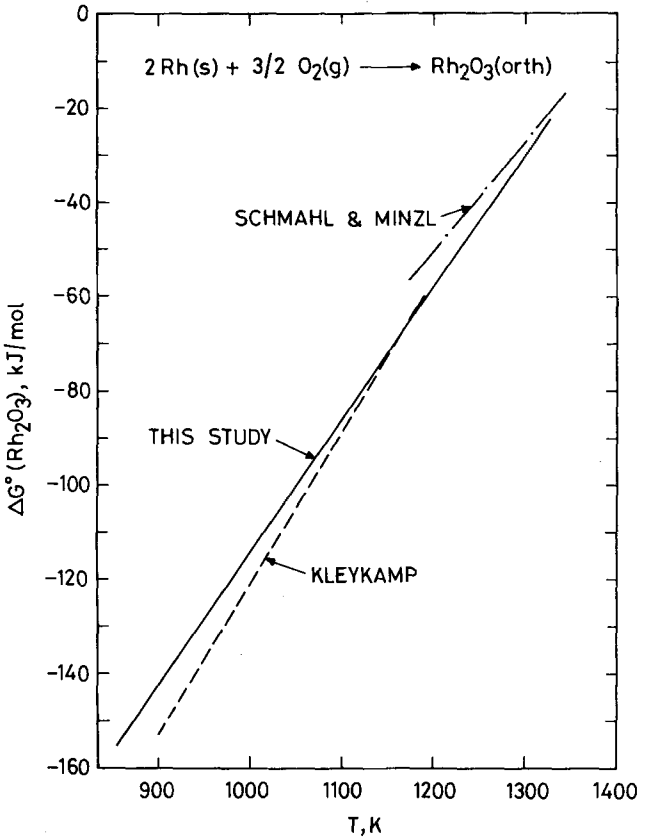

Fig. 8—Comparison of the standard Gibbs free energy of formation of Rh_2O_3 obtained in this study with data reported in the literature.

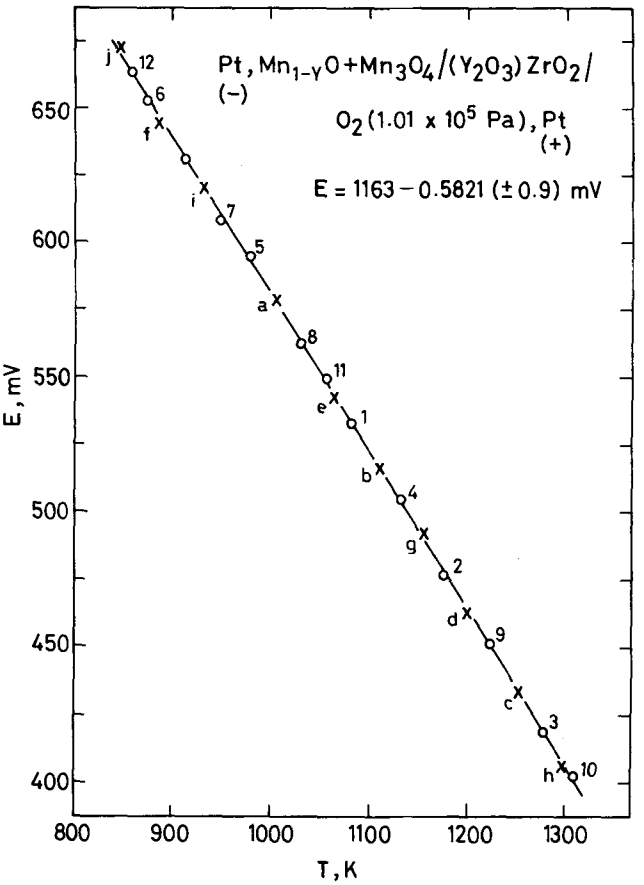

Fig. 9—Dependence of the emf of cell [6] on temperature.

$$\Delta\mu_{O_2}(Mn_{1-y}O + Mn_3O_4) = -448{,}900 + 224.7T\ (\pm 400)\ \text{J mol}^{-1} \quad [29]$$

The value of the nonstoichiometric parameter Y in Mn_{1-y} is ~0.01 at 1100 K, based on the measurements of Bransky and Tallan,[27] Picard and Gerdanian,[28] and Keller and Dieckmann.[29] If this nonstoichiometry is neglected, the reaction defining the oxygen potential can be approximated as

$$6\ \text{'MnO'} + O_2 \rightarrow 2\ Mn_3O_4 \quad [30]$$

The standard free energy change for the reaction obtained in this study is compared in Figure 10 with values reported by earlier investigators. The results of this study are in good agreement with the measurements of Charette and Flengas[8] and Blumenthal and Whitmore,[9] but differ somewhat from the data suggested by Huebner and Sato[11] and Chou,[12] especially at lower temperatures. The agreement between the results of this study, Charette and Flengas,[8] and Blumenthal and Whitmore[9] is encouraging, especially since three different reference electrodes—O_2 (the study), Ni + NiO (Charette and Flengas), and Fe + FeO (Blumenthal and Whitmore)—are used in the separate investigations. The second law enthalpy change for Reaction [30] at 298.15 K obtained in this study is −455.5 (±2.5) kJ mol^{-1}, using heat capacities for Mn_3O_4 suggested by Robie and Hemingway[30] and data for MnO and O_2 from Pankratz.[26] The low-temperature calorimetric studies of Robie and Hemingway[30] have significantly changed data for Mn_3O_4, Mn_2O_3, and MnO_2. The "third law" enthalpy change for Reaction [30] evaluated from the present emf measurements, using the new thermal functions for Mn_3O_4[30] and evaluated functions for MnO and O_2[26] is −458.1 (±0.5) kJ mol^{-1}. This compares with the value of −463.9 (±3.6) kJ mol^{-1} calculated from the solution calorimetric results of Shomate[31] and Southard and Shomate.[32] Shomate[31] used two methods to evaluate ΔH_f° (298.15 K) for Mn_3O_4. If one of the results of Shomate for Mn_3O_4 is corrected using the newer, more accurate values listed by Wagman *et al.*[33] for the enthalpy of formation of HI (aq), the enthalpy of formation becomes −1383.45 kJ mol^{-1} at 298.15 K. The results of the second method used by Shomate[30] remain unchanged. The average value becomes −1385.45 kJ mol^{-1}. The calorimetric enthalpy change for Reaction [30] then becomes −459.6 kJ mol^{01} at 298.15 K, in better agreement with the third law value deduced from the present measurements. The difference of 2.6 kJ mol^{-1} between the second law and third law enthalpy change for Reaction [30] at 298.15 K obtained in this study may in part be due to the small nonstoichiometry of $Mn_{1-Y}O$ which is a function of temperature.

5. *Oxygen potential diagram for the system Mn-Rh-O*

An oxygen potential diagram for the system Mn-Rh-O at 1273 K, composed from the results of the present

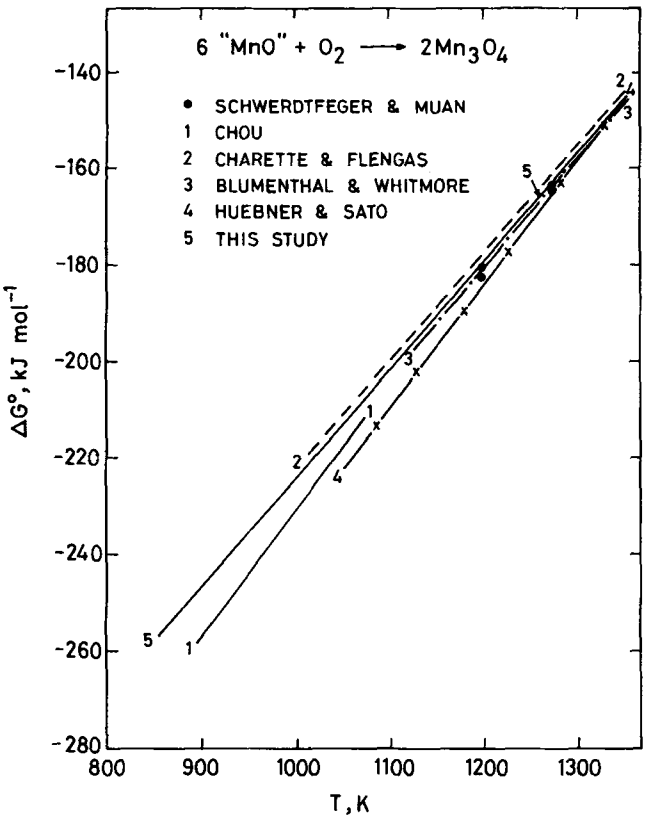

Fig. 10—Comparison of the oxygen chemical potential for the coexistence of $Mn_{1-y}O$ and Mn_3O_4 obtained by different investigators.

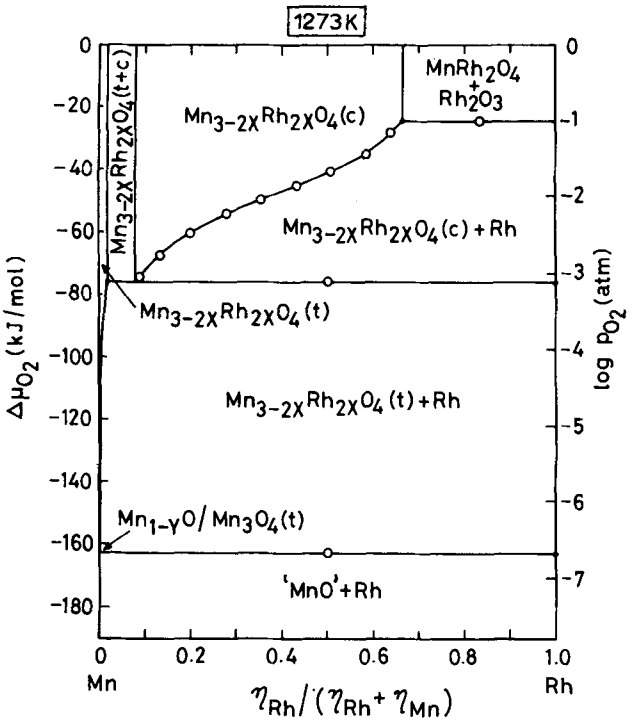

Fig. 11—Oxygen potential diagram for the system Mn-Rh-O at 1273 K.

study, is shown in Figure 11. The composition of phases is represented by cationic fraction, $\eta_{Rh}/(\eta_{Rh} + \eta_{Mn})$, where η_i denotes moles of component i. Since oxygen is not included in the composition parameter, information on oxygen nonstoichiometry cannot be displayed on the diagram. Nevertheless, the diagram provides useful information on the oxygen potential range for the stability of various phases. The diagram is complementary to the Gibbs triangle representation of phase relations in a ternary system, where phase compositions can be clearly identified. All the topological rules of construction for conventional temperature-composition phase diagrams are applicable to the oxygen potential diagram shown in Figure 11.

When three condensed phases and a gas phase are in equilibrium in a ternary such as Mn-Rh-O, the system is monovariant; at a fixed temperature, the three condensed phases coexist only at a unique partial pressure of oxygen. The three-phase equilibria are therefore represented by horizontal lines on the diagram. The low oxygen partial pressure boundary for the stability of cubic $Mn_{3-2x}Rh_{2x}O_4$ at 1273 K ranges from 9.48×10^3 Pa for $X = 1$ to 76 Pa for $X = 0.12$. Tetragonal Mn_3O_4 containing a small amount of dissolved $MnRh_2O_4$ is stable up to 2.07×10^{-2} Pa. Equilibria at very low oxygen potentials between alloys and MnO are not shown in Figure 11, since thermodynamic properties of Mn-Rh alloys required for the calculation are not available. Similar diagrams at other temperatures can be readily calculated from the thermodynamic data obtained in this study.

IV. SUMMARY

A study of phase relations in the system Mn-Rh-O indicates that only one ternary compound, $MnRh_2O_4$, is present at 1273 K. There is an extensive solid solution between Mn_3O_4 and $MnRh_2O_4$. The structure of the solid solution is tetragonal near the Mn_3O_4 corner and cubic for the rest of the compositions. The oxygen potential corresponding to the coexistence between the solid solution and metallic Rh is measured as a function of temperature, using a solid-state emf technique. A special design of the cell is developed for the measurements of two-phase equilibria in a ternary system, with 1 degree of freedom at constant temperature. A nonpolarizable reference electrode is employed in conjunction with a buffer electrode placed between the reference and measuring electrodes. The buffer electrode, maintained at approximately the same oxygen chemical potential as the measuring electrode, absorbs the semipermeability flux of oxygen between reference and measuring electrodes. The technique is validated by measurement of oxygen potential of MnO + Mn_3O_4 and Rh + Rh_2O_3 systems, which are invariant at constant temperature.

Using a new form of the Gibbs–Duhem equation and the measured oxygen partial pressures for the two-phase equilibria between Rh and $Mn_{3-2x}Rh_{2x}O_4$, activities in the solid solution and Gibbs energy of formation of $MnRh_2O_4$ are derived. The relative free energy of mixing is given by

$$\Delta G^M = 2435\, X\,(1 - X) + 2RT\,[X \ln X + (1 - X) \ln (1 - X)]\ \text{J mol}^{-1}$$

The activities in Mn_3O_4 – $MnRh_2O_4$ cubic solid solution

exhibit negative deviations from Raoult's law. The standard free energy of formation of the cubic spinel $MnRh_2O_4$ from component oxides MnO with rock salt and Rh_2O_3 with orthorhombic structures can be expressed by the equation

$$\Delta G^\circ = -49{,}680 + 1.56T\ (\pm 500)\ \text{J mol}^{-1}$$

An oxygen potential diagram for the Mn-Rh-O system at 1273 K is composed from the results of this study.

REFERENCES

1. N.G. Schmahl, D. Hennings, and W. Schneider: *Z. Phys. Chem. (Wiesbaden)*, 1969, vol. 63, pp. 125-31.
2. K.T. Jacob and T. Mathews: *J. Mater. Chem.*, 1991, vol. 1, pp. 545-49.
3. *Binary Alloy Phase Diagrams*, T.B. Massalski, ed., ASM, Metals Park, OH, 1990, vol. 3, pp. 2593-95.
4. K.T. Jacob and J.H.E. Jeffes: *High Temp.-High Pressures*, 1972, vol. 4, pp. 177-82.
5. J.N. Pratt: *Metall. Trans. A*, 1990, vol. 21A, pp. 1223-50.
6. J. Fouletier, P. Fabry, and M. Kleitz: *J. Electrochem. Soc.*, 1976, vol. 123, pp. 204-13.
7. G.M. Kale and K.T. Jacob: *Metall. Trans. B*, 1992, vol. 23B, pp. 57-64.
8. G.G. Charette and S.N. Flengas: *J. Electrochem. Soc.*, 1964, vol. 115, pp. 796-804.
9. R.N. Blumenthal and D.H. Whitmore: *J. Am. Ceram. Soc.*, 1961, vol. 44, pp. 508-12.
10. K. Schwerdtfeger and A. Muan: *Trans. AIME*, 1967, vol. 239, pp. 1114-19.
11. J.S. Huebner and M. Sato: *Am. Mineral.*, 1970, vol. 55, pp. 934-52.
12. I.M. Chou: *Am. Mineral.*, 1978, vol. 63, pp. 690-703.
13. H. Kleykamp: *Z. Phys. Chem. (N.F.)*, 1969, vol. 67, pp. 277-83.
14. N.G. Schmahl and E. Minzl: *Z. Phys. Chem. (N.F.)*, 1964, vol. 41, pp. 78-96.
15. K.T. Jacob and J.H.E. Jeffes: *Trans. Inst. Min. Metall., Section C*, 1971, vol. 80, pp. C181-C189.
16. K.T. Jacob and T. Mathews: *Ind. J. Tech.*, 1990, vol. 28, pp. 413-27.
17. R. Akila, A.K. Shukla, and K.T. Jacob: *Bull. Mater. Sci.*, 1986, vol. 8, pp. 453-65.
18. M. Lundberg and E. Rosén: *J. Am. Ceram. Soc.*, 1992, vol. 75, pp. 1452-57.
19. C. Mallika, R. Pankajavalli, and O.M. Sreedharan: *Electrochim. Acta*, 1986, vol. 31, pp. 885-86.
20. R. Metselaar, R.E.J. Van Tol, and P. Piercy: *J. Solid State Chem.*, 1981, vol. 38, pp. 335-41.
21. J.D. Dunitz and L.E. Orgel: *J. Phys. Chem. Solids*, 1957, vol. 3, pp. 318-23.
22. K.T. Jacob and C.B. Alcock: *Metall. Trans. B*, 1975, vol. 6B, pp. 215-21.
23. G. Blasse: *Philips Res. Rep.*, 1964, Suppl. 3.
24. R.D. Shannon and C.T. Prewitt: *Acta Crystallogr.*, 1969, vol. B25, pp. 925-46.
25. R.D. Shannon and C.T. Prewitt: *Acta Crystallogr.*, 1970, vol. B26, pp. 1046-48.
26. L.B. Pankratz: *Thermodynamic Properties of Elements and Oxides*; U.S. Bureau of Mines Bull. 672, U.S. Government Printing Office, Washington, DC, 1982, pp. 229-36.
27. I. Bransky and N.M. Tallan: *J. Electrochem. Soc.*, 1971, vol. 118, pp. 788-93.
28. C. Picard and P. Gerdanian: *J. Solid State Chem.*, 1974, vol. 11, pp. 190-202.
29. M. Keller and R. Dieckmann: *Trans. Jpn. Inst. Met.*, 1983, vol. 24, pp. 650-51.
30. R.A. Robie and B.S. Hemingway: *J. Chem. Thermodyn.*, 1985, vol. 17, pp. 165-81.
31. C.H. Shomate: *J. Am. Chem. Soc.*, 1947, vol. 69, pp. 218-19.
32. J.C. Southard and C.H. Shomate: *J. Am. Chem. Soc.*, 1942, vol. 64, p. 1770.
33. D.D. Wagman, W.H. Evans, V.B. Parker, R.H. Schumm, I. Halow, S.M. Bailey, K.L. Churney, and R.L. Nuttall: National Bureau of Standards Tables of Chemical Thermodynamic Properties, *J. Phys. Chem. Ref. Data*, 1982, vol. 11, Suppl. 2, pp. 1-394.